

Characterizing driver heterogeneity and reproducing it within traffic simulation

Makridis^a, M., Anesiadou^c, A., Mattas^b, K., Fontaras^b, G., Ciuffo^{b,1}, B.

^aETH Zürich, Institute for Transport Planning and Systems (IVT), Zürich, CH

^bEuropean Commission – Joint Research Centre., Ispra (VA), Italy

^cFINCONS Group, 20871 Vimercate, Italy. The work by this authors has been carried out for the European Commission Joint Research Centre

Abstract

Drivers' heterogeneity and the broad range of vehicle characteristics are primarily responsible for the stochasticity observed in road traffic dynamics. Understanding the differences in human drivers and reproducing observed behaviours in microsimulation has attracted significant attention lately. The present study proposes a novel framework to analyse observed vehicle trajectories and provide understanding of the driver's driving style. The paper discusses the inability of instantaneous acceleration measurements to characterise the aggressiveness of a driver and proposes a novel metric called Independent Driving Style (IDS) that is independent of the vehicle dynamics and the current speed. The proposed metric is therefore suitable for comparisons of different drivers. Furthermore, it builds on an existing, well documented vehicle dynamics and driver model and proposes an update for stochastic driver simulation. The proposed framework is validated and assessed through a sizeable experimental campaign with 20 drivers using interchangeably the same vehicle for one year. Results demonstrate the ability to capture inter and intra-driver heterogeneity with lognormal distributions of the instantaneous IDS values of the drivers. Intra-driver heterogeneity is captured based on median, 25th percentile and 75th percentile from each driver's distribution. Classification of drivers into three prevalent groups (dynamic, ordinary and mild drivers) is adequate to capture the inter-driver heterogeneity and facilitates easier driver-fleet reproduction in large-scale microscopic simulation software. Inter-driver heterogeneity is quantified using descriptive statistics, i.e. the interquartile range per driver. Finally, a new stochastic car-following model using the driver distributions is proposed and demonstrated in the paper through simulation for the three groups of drivers. Similar to real-world observations, an aggressive driver does not accelerate faster than a mild one at all instances. However, their overall behavioural difference should be apparent across a large number of observations. Simulation results demonstrate the ability of the proposed model to infer stochastically such behavioural characteristics.

1 Introduction

Variability in the behaviour of human drivers and vehicle dynamics is responsible for the emergence of stochastic patterns in the way vehicles move and interact. Commercial fleets are composed of many heterogeneous vehicles in terms of power dynamics, powertrains and vehicle manufacturers. Furthermore, stochasticity in vehicle movement under similar conditions is present even for the same vehicle brand and model due to heterogeneous human driving behaviours. For the longitudinal vehicle movement, which is the topic of this work, dynamic drivers are (in principle) faster on free-flow or keep shorter time gaps while on car-following than mild drivers. On a macroscopic scale, this heterogeneity has been linked to the evolution of several traffic-related phenomena such as capacity drop, traffic hysteresis, traffic oscillations, and stop and go waves, to name a few (Chen et al., 2014; Huang et al., 2018; Laval and Leclercq, 2010; Saifuzzaman et al., 2017; Zheng et al., 2011).

¹ Corresponding author. E-mail: Biagio.CIUFFO@ec.europa.eu

Several attempts to characterize driver heterogeneity have been carried out in the past decades. In general, research efforts have so far focused on the variability in the behavior of the same driver, called intra-driver heterogeneity (Berthume et al., 2018; Huang et al., 2018; Wang et al., 2010), or of different drivers, called inter-driver heterogeneity (Taylor et al., 2015), or both (Ossen and Hoogendoorn, 2011). With the advent of automated driver assistance systems, such as Adaptive Cruise Control (ACC), a reduction (at least) in driver heterogeneity and most probably also in observed vehicle dynamics is expected (Makridis et al., 2021). This gives an additional motivation to gain a deeper understanding and accurate description of observed driving behaviors, as this would facilitate meaningful comparative studies between human and automated drivers (Calvert and van Arem, 2020; Zhao et al., 2020). The first goal of the present work is therefore to analyse both inter and intra-driver heterogeneity in a concise way, providing a robust indicator for quantitative comparisons between different drivers.

On the simulation side, traffic microsimulation software reproduce individual vehicle movement aiming at highlighting complex traffic dynamics. Within microscopic traffic models, car-following models reproduce the longitudinal driving task. New models are continuously being proposed to overcome the limitations of existing ones including the capability to properly handle the effect of drivers' heterogeneity. However, this is often achieved in a stochastic way, without a direct link with any physical mechanism that includes the variability in the vehicle dynamics and the driver behaviour (Laval et al., 2014; Ngoduy et al., 2019; Treiber et al., 2006; Treiber and Kesting, 2013).

In particular, existing models cannot reproduce vehicle and driver micro-dynamics realistically when the vehicle moves under free-flow conditions, leading to unrealistic accelerations and fuel consumption estimates (Ciuffo et al., 2018). This has not been the subject of major research efforts as the free-flow driving component of car-following models has always been considered of secondary importance in the description of traffic dynamics. However, an increasing number of works has recently highlighted the importance of free-flow behaviour even under congested traffic conditions (Laval et al., 2014). Under such conditions, in fact, there is a significant variation in the inter-vehicle distances due to high driver heterogeneity. Large inter-vehicle distances, often called free-flow pockets, emerge and, during such pockets, drivers behave closer to free-flow conditions (Makridis et al., 2020a). Building on the findings of these recent studies, the present paper also proposes a novel way to simulate driver heterogeneity by stochastically integrating it in the MFC model (Makridis et al., 2019), which explicitly accounts for the dynamics of vehicle powertrain. An implementation of the MFC model on Python programming language is openly available online².

The power capabilities of a vehicle remain mostly constant throughout its lifetime. However, this is not the case for the individual behaviour of each driver. Usually, driving behaviour can be influenced by several stochastic factors (intra-driver heterogeneity), such as drivers' mood, the time of the day, the traffic state, the weather and many others (Hoogendoorn et al., 2011). So, the ability to create a model that captures a driver's behaviour, assuming enough observations, can be achieved only through a stochastic process characterized by an average behaviour and an expected variance. In microsimulation software and studies, this process is modelled through a random variance in the instantaneous acceleration of each vehicle agent. However, we argue that acceleration is not enough to characterise a driver, because the power dynamics are not uniform across any vehicle's speed range. Most vehicles with internal combustion engines have high power capabilities and thus high acceleration potential at low speeds and much lower in high speeds. Therefore, considering only the acceleration without taking into account the instantaneous speeds can produce misleading conclusions for the driver's aggressiveness. For example, let us imagine an aggressive driver accelerating from an initial speed of 10km/h and the same vehicle-driver system accelerating from an initial speed of 100km/h. In the first case, the observed instantaneous accelerations will probably be much larger than in the second case. The reason is that the vehicle's nominal acceleration capacity reduces with

² <https://pypi.org/project/co2mpas-driver/>

the increase in the speed. In this work, we therefore also discuss about the inability of acceleration as a metric to describe the driver aggressiveness in different speeds and thus to provide fair quantitative comparisons between drivers that drive in different traffic conditions. To solve this issue, we introduce a novel metric that considers acceleration as a function of speed to facilitate vehicle-independent and speed-independent driver comparisons.

The paper is structured as follows: Section 2 presents the proposed framework, the updated model and the experimental campaign, Section 3 presents the results and Section 4 the conclusions.

2 Methodology

We propose a methodological approach to analyse a driver's behaviour based on observed vehicle trajectories. A discussion on the properties and limitations of instantaneous accelerations for driver behaviour understanding is performed. A novel instantaneous metric is proposed based on the variation of the driver's acceleration. The developed metric that is called Independent Driving Style (IDS) is independent of the vehicle specifications and the observed speed, thus facilitating objective comparisons between different drivers. Assuming enough observations that capture all the possible behaviours of a driver (large datasets), a distribution of IDS values is produced. Such distribution can be perceived as the driver's behavioural fingerprint. In the second part of the methodology, this work focuses on the reverse problem: the microsimulation of an observed driver, given the estimated PDF of his IDS values. A high-level schematic representation of the proposed framework is illustrated in Figure 1. The different components are discussed in the next sections.

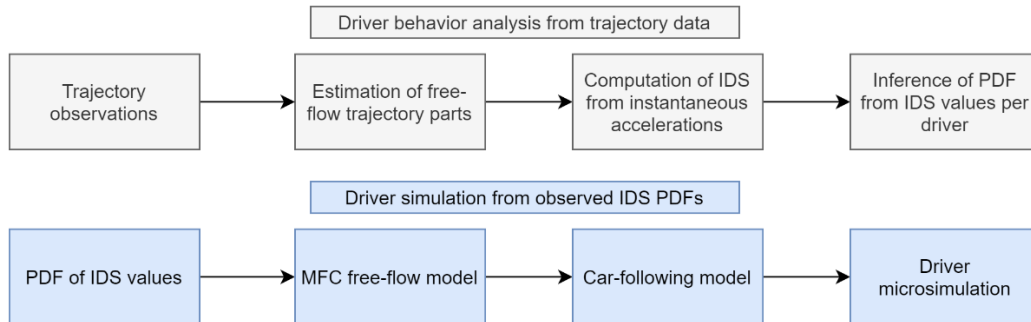


Figure 1. High-level schematic representation of the proposed framework. The top part refers to driver analysis; the lower part to driver simulation.

2.1 Independent Driving Style (IDS)

The behavioural differences between drivers are more prominent when other drivers or obstacles do not constrain them. Such conditions refer to free-flow traffic conditions when there is no vehicle in front or the leading vehicle is far enough to allow unconstrained driver action (as in the case of the appearance of free-flow pockets in congested traffic conditions). However, in empirical datasets used to characterize the behaviour of an individual driver, information about the presence of a leading vehicle is not always given. Even with the presence of the leading vehicle, there is no concrete threshold regarding whether the driver is constrained by it or not. Therefore, we adopt an indirect way to estimate free-flow conditions. The idea is that under unconstrained driving, the drivers accelerate sharp enough to go from a lower to a higher speed relatively quickly. However, this is not possible when they are constrained by a leading vehicle, a traffic light or other obstacles. So, initially, we attempt to detect small trajectory parts with sharp accelerations.

The first step in the methodology is therefore to analyse trajectory data and extract the parts that correspond to sharp-enough accelerations to be possibly linked with free-flow conditions.

2.1.1 Estimation of free-flow trajectory observations

From trajectory data, it is relatively easy to detect acceleration events, namely those time intervals in which a vehicle accelerates from a starting speed to a higher one (with a speed jump of Δv) without interruptions. If the duration of this acceleration event, namely w , is short enough (sharp acceleration), and the speed jump Δv is large enough, then we can do a logical assumption that this vehicle is under free-flow conditions. Therefore, there is a correlation between Δv and w in order to identify an acceleration event with potential free-flow conditions. The higher the Δv , the longer the acceptable w can be.

Consequently, the acceleration events in trajectory data can be detected through sequential local extrema (maxima and minima) on the speed profile. For each event, the speed jumps Δv and duration w are recorded. We assume that each acceleration event can correspond either to free-flow or the following conditions. In order to implement such an algorithm, we need the two threshold values Δv_{th} and w , that will differentiate the free-flow from car-following trajectory parts.

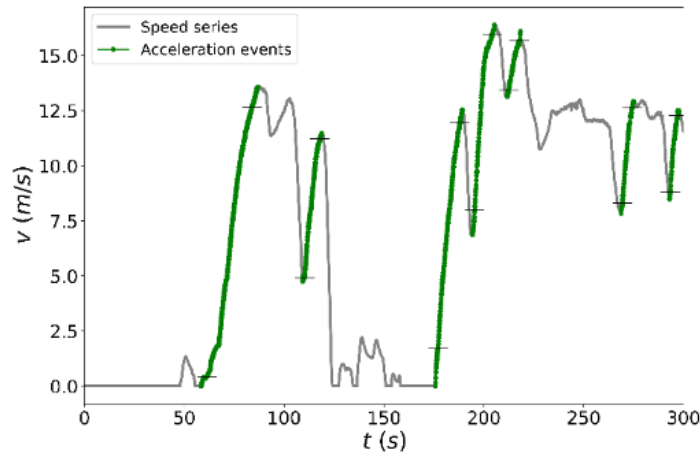


Figure 2. Example of acceleration events from measured speed profiles.

First, we apply a simple local min/max algorithm to detect all possible acceleration events (matching sequential local minima and local maxima). Then, the idea is to filter only those that most probably correspond to free-flow conditions. For that purpose, under the “reductio ad absurdum” logic, we use the trajectory data from real-world car-following campaigns (Makridis et al., 2021) that are designed for vehicle platoons, thus trajectory data primarily for car-following conditions. In the experiments, the leading vehicle performs speed drops to study the platoon's stability properties. Primarily the data refer to car-following, but free-flow pockets are expected to appear during deceleration perturbations. Consequently, for each detected event we record the Δv values and their duration. Then heuristically, we setup the Δv_{th} value to the 75th percentile of our observations. Since there is high variability in the duration of acceleration events, in this approach, we split the Δv values in four clusters according to their duration, i.e. shorter than 7s, 7s-12s, 12s-17s and longer ones. We can imagine that there are possibly more efficient ways for identification of Δv_{th} but this is outside this paper's main contributions. An example of estimated free-flow acceleration events is shown in Figure 2.

2.1.2 Acceleration as a measure for driver characterisation

The instantaneous acceleration is often used in the literature to characterise drivers' aggressiveness (Hamdar et al., 2015; Hoogendoorn et al., 2011; Taylor et al., 2015). However, instantaneous acceleration as metric, it can be misleading for comparative analysis when the drivers use vehicles with very different power

capabilities or the observations refer to different traffic conditions or driving environments. To explain this concept, Figure 3 has been derived through modelling from available experimental data and describes the acceleration over speed domain for one specific vehicle. In particular, in Figure 3 the cyan line depicts the acceleration potential of the vehicle across the whole speed range. The yellow line shows the maximum common acceleration values observed at each given speed, and similar the orange line shows the minimum common deceleration values observed at each given speed for the specific vehicle. These three lines define four regions, namely Regions A, B, C and D.

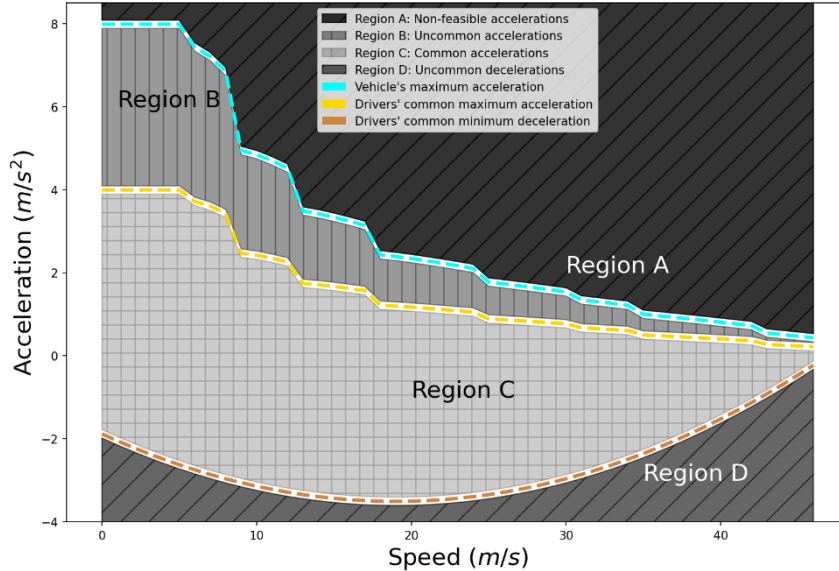


Figure 3. The unrealistic, feasible and common acceleration-speed domain (model representation) for the vehicle used in the experimental campaign described in Section 2.4.

Region C contains acceleration values that are most frequently observed in observations. The union between Region B and C describes the domain of plausible values, while Regions A and D include unrealistic acceleration values that the vehicle cannot deliver due to power or other limitations. From the figure, it is possible to understand the unsuitability of acceleration to characterise driving aggressiveness for the following reasons. First, when two vehicles have a significant difference in power capabilities, their acceleration at a given speed is not comparable. Second, a driver adapts to the vehicle capabilities. Therefore, it is unfair to characterise a driver of a sport car as more aggressively only because the car can produce higher acceleration than conventional ones. Third, the acceleration response of commercial vehicles is not uniform across their speed range. It is obvious from Figure 3 that the maximum possible acceleration for speeds around 10m/s (urban) is higher than 4m/s^2 , while for speeds around 30m/s (freeway) is around 1m/s^2 . It is therefore unfair to compare drivers observed with acceleration values measured on high speeds with those measured on low speeds.

In order to address this problem, in the present work we transform the instantaneous acceleration values to become independent of the vehicle and independent of the speed. We achieve this in a two-step methodology described in the next sections.

2.1.3 Vehicle-independent acceleration values

Transformation of instantaneous acceleration values to vehicle-independent ones is possible if we know the vehicle specifications. Assuming known vehicle specifications we model the acceleration capacity of a

vehicle, that is, the maximum possible acceleration that the vehicle can deliver at a given speed. The idea is to express the acceleration as a rate of the vehicle's acceleration potential at the given speed.

There are several models of this type in the literature (Fadhloun and Rakha, 2020; Makridis et al., 2019; Rakha et al., 2004, 2012). Here, we use the MFC model proposed in (Makridis et al., 2019). The employed model has been extended also for electric vehicles that demonstrate different power distribution across speed range (He et al., 2020).

Using the MFC model we construct the acceleration capacity function of the vehicle, namely $a_{cp}(v)$ (i.e. cyan line in Figure 3), where v is the instantaneous speed. It should be noted that $a_{cp}(v)$ is also a function of the current gear, which is computed based on the work of (Fontaras et al., 2018). Then we express the instantaneous acceleration a as a rate of $a_{cp}(v)$:

$$ds = \frac{a}{a_{cp}(v)} \quad (1)$$

As it can be perceived, the ds quantity is related to the acceleration but it is independent of the vehicle power capabilities. In generalised studies, the reader can use average acceleration potential functions based on average vehicle performance in commercial fleets to avoid the need for knowledge of each individual vehicle's specifications.

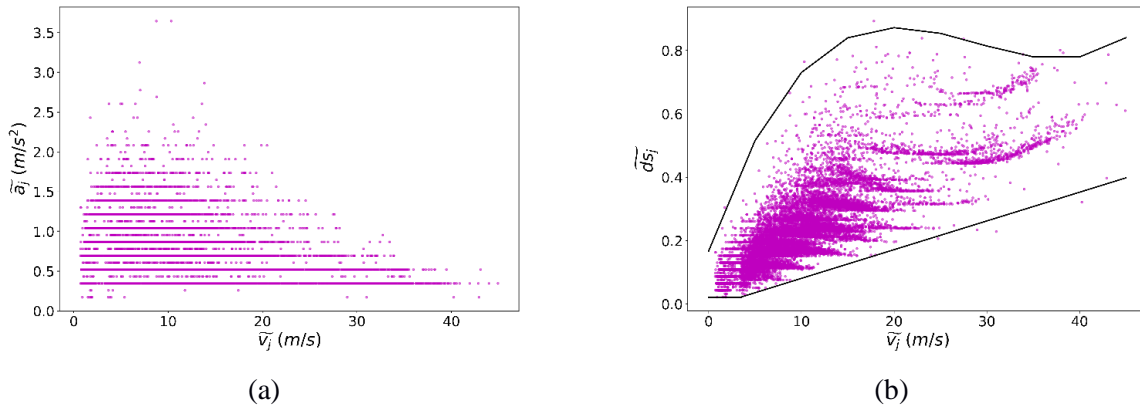


Figure 4. a) Median acceleration per event versus median speed per event plot, b) Median ds per event versus median speed per event plot. Data refer to 20 observed drivers.

In the remaining part of the driver analysis, we perform the logical assumption that a driver does not change his/her driving behaviour during a single acceleration event. That is why instead of concentrating at instantaneous acceleration, we continue our analysis based on the median acceleration/speed values observed during a detected acceleration event. In this way, the characterization is also less affected by measurement noise (the median value is not sensitive to outliers), which is usually significant for the vehicle acceleration, especially when computed by differentiation of the speed or double differentiation of the position (Punzo et al., 2011).

Figure 4 is an intuitive demonstration of this new vehicle-independent metric. For each acceleration event (estimated for free-flow conditions), Figure 4a shows the median acceleration value of the event and the corresponding median speed based on real-world measurements. It is clear, as noted before that the observed acceleration values are much higher in low speeds than in high speeds. This plot refers to a large pool of drivers, driving unconstrained to various networks (freeway or urban) and traffic conditions (free-flow or congested). Figure 4b shows the proposed ds values (median per event) for all the drivers. The black lines inscribe the operational domain of possible ds values in real-world driving conditions. In other words,

assuming that we have enough observations, the observed acceleration values of any new driver should fall inside the domain that the black lines inscribe.

2.1.4 Speed-independent acceleration values

We discussed how ds is a vehicle-independent metric but the correlation with speed remains. It can be seen in Figure 4a that the observed accelerations are higher at lower speeds and lower at higher speeds. In contrast, the observed ds values are lower in low speeds and higher in high speeds. Consequently, the goal here is to transform the observed ds values to become speed independent. We employ a simple process to achieve this. First we derive two equations that describe the black lines observed in Figure 4b, namely $f_{min}(v)$ and $f_{max}(v)$. The fitted curves are reported in Appendix Part A for reproducibility of the proposed study. Secondly we express the observed ds values as a rate of the operational domain that f_{min} and f_{max} describe as follows:

$$ids = \frac{ds - f_{min}(v)}{f_{max}(v) - f_{min}(v)} \quad (2)$$

Where ids is called Independent Driving Style (IDS), ds derives from Eq.1 and v is the observed speed. For the sake of demonstration in this work, we assume that the $f_{min}(v)$ and $f_{max}(v)$ have global validity. In other words, we assume that our pool of drivers is large enough to describe all possible driving behaviors, or our dataset is large-enough to capture all possible networks and traffic conditions. Consequently, in real-world application, the $f_{min}(v)$ and $f_{max}(v)$ need to be updated as new observations arrive in order to describe the drivers' operational domain properly.

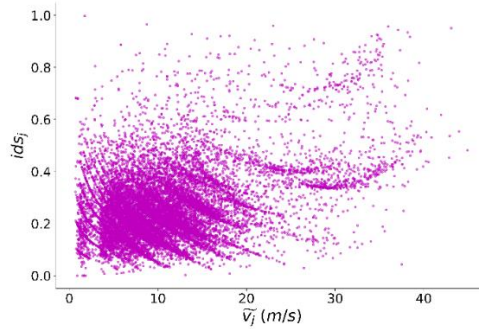


Figure 5. Uniform distribution of IDS values across the whole speed range. Data refer to 20 observed drivers (j denotes the ID of an acceleration event).

Figure 5 shows that derived IDS metrics (median values per event) and the corresponding observed speeds (median values per event) and demonstrates that it can achieve almost all possible values in the domain $[0,1]$ across the whole speed range. More details on the correlation between ids_j with \tilde{v}_j , where j denotes the ID of an acceleration event, are presented in Appendix Part B.

2.2 Driver characterisation using distributions of IDS values.

Assuming that enough observations are available for a driver across different vehicles, speeds, networks and traffic conditions, we derive his/her histogram. The notion behind this is that human drivers do not drive in a uniform driving style all the time. As mentioned above, human drivers' aggressiveness may vary, depending on an undefined number of stochastic factors such as their mood, the time of the day, the traffic state, the weather and many others. However, we argue that every driver has different distribution of possible behaviours. There are differences that sometimes might not be visible at micro scale, i.e. during a short trip, but across their driving life, these differences become apparent.

In order to facilitate analytical comparison, we then approximate the derived histograms with probability density functions (PDF). In this work, we assume and validate our assumption that driver IDS observations follow a lognormal PDF. Each fitted PDF can be thought as the driver’s behavioural fingerprint.

2.3 Stochastic microsimulation of observed drivers

Here, we propose a novel way to perform such a simulation process. The goal here is to incorporate the PDFs into the simulation process. In order to sample from a PDF and transform this value back to a plausible acceleration, we use the following equation:

$$ds = ids \cdot (f_{max}(v) - f_{min}(v)) + f_{min}(v) \quad (3)$$

Equation 3 is the reverse operation from Eq.2, where ids is the sample from the driver’s PDF, f_{min} and f_{max} are functions over speed as explained above and v is the instantaneous speed. Consequently, one can easily extract instantaneous acceleration as follows:

$$a = [ds \cdot (f_{max}(v) - f_{min}(v)) + f_{min}(v_t)] a_{cp}(v) \quad (4)$$

The proposed free-flow model builds on the MFC model by substituting the constant driving style parameter with a dynamic value inferred from PDF of the driver. Previous work by the authors (Makridis et al., 2020a) proved that the original MFC model (with constant driving style per driver) within the framework of the LWR model, successfully reproduces macroscopically-observed traffic patterns. More specifically, the MFC-LWR model reproduces the concave growth pattern for the speed standard deviation on perturbations, traffic oscillations of various frequencies and amplitudes and leads to more accurate fuel consumption estimates. Therefore, this work skips this part and focuses on the properties that the proposed model introduces on the free-flow part only. Finally, we cluster the drivers into three main styles, mild, normal and aggressive. The idea behind this simplification is to facilitate incorporation of this work’s outputs in large-scale microsimulation studies, since the modelling of each individual behaviour would be extremely challenging.

2.4 Experimental campaign

In order to validate the proposed methodology we conducted an experimental multi-driver campaign, driving the same vehicle under different driving conditions. A dataset was created from individual trajectories of 20 drivers collected over a period of 12 months. The vehicle used in the test campaign is a 2.0L diesel C-segment passenger car, equipped with automatic transmission (9 gears), leased for 12 months (second half of 2016 and the first half of 2017). The experiments were conducted by the Joint Research Centre of the European Commission as part of the OpenACC initiative³ (Makridis et al., 2021). The dataset consists of more than 10.000 km driven by 20 drivers using the same vehicle. During the experimental campaign, every two weeks, the vehicle was assigned to a volunteer driver, who was free to use it as a personal vehicle without any restriction on the frequency of usage, the driving style, the fuel consumption or the route choice. For additional information on the test campaign, the reader can also refer to the corresponding publication (Pavlovic et al., 2020).

Table 1 provides an overview of the dataset with distance and trips’ time duration per driver. Time duration refers to actual driving time without long pauses. The differences in the number of driven kilometres or hours travelled can be explained by the fact that there was no restriction or guidance on how each driver uses the vehicle. Additionally, this table shows the number of acceleration events detected for each driver, along with the distance in km covered during those events.

Table 1. Basic statistics of the trips per driver.

³ <http://data.europa.eu/89h/9702c950-c80f-4d2f-982f-44d06ea0009f>

Driver	Total kms	Total hours	Free-flow events number	Events (km)	Driver	Total kms	Total hours	Free-flow events number	Events (km)
D1	250	8	715	117	D11	1056	14	420	171
D2	669	9	447	129	D12	119	4	456	55
D3	1973	39	2807	538	D13	1039	21	1401	307
D4	300	4	223	46	D14	1189	20	1009	295
D5	1055	14	482	134	D15	311	8	548	122
D6	45	2	176	20	D16	2581	35	942	405
D7	166	3	151	58	D17	288	7	632	118
D8	442	13	1054	150	D18	183	7	614	77
D9	310	7	619	111	D19	303	6	345	68
D10	174	6	481	71	D20	1424	19	1139	297

3 Results

This section presents the results of the proposed methodology to showcase intra- and inter-driver heterogeneity, as well as simulate specific driver profiles.

3.1 Inferring the PDF distribution per driver

In the methodology section, IDS was identified as a normalised metric, independent of the speed and the vehicle's powertrain, necessary to perform an objective comparison between different drivers. The IDS values per driver were derived from the median accelerations observed during the acceleration events derived using the methodology described in Section 2. The derivation of lognormal PDF was assessed using the Kolmogorov-Smirnov (K-S) test, which is a nonparametric statistical test of the equality of one-dimensional probability distributions. K-S is used here as a goodness of fit test to compare the observed estimated PMF (histogram) with the continuous reference-fitted PDF.

In Figure 6, the empirical distributions of observed IDS values per driver are presented with the y-axis denoting probability density. The lognormal distribution has been indeed mentioned in the literature as suitable for the description of human behaviors. Gualandi and Toscani studied the connection between human behavior and lognormal distribution also considering cases of modelling drivers in traffic (Gualandi and Toscani, 2019). Furthermore, Antoniou et al. (Antoniou et al., 2002) concluded that the aggregation of traffic measurements forms a statistical distribution, which is quite accurately described by a lognormal distribution. The goodness of fit test results based on the K-S method are reported in the Appendix Part C. The parameters of the lognormal PDFs for all drivers are given for reference in Appendix Part D.

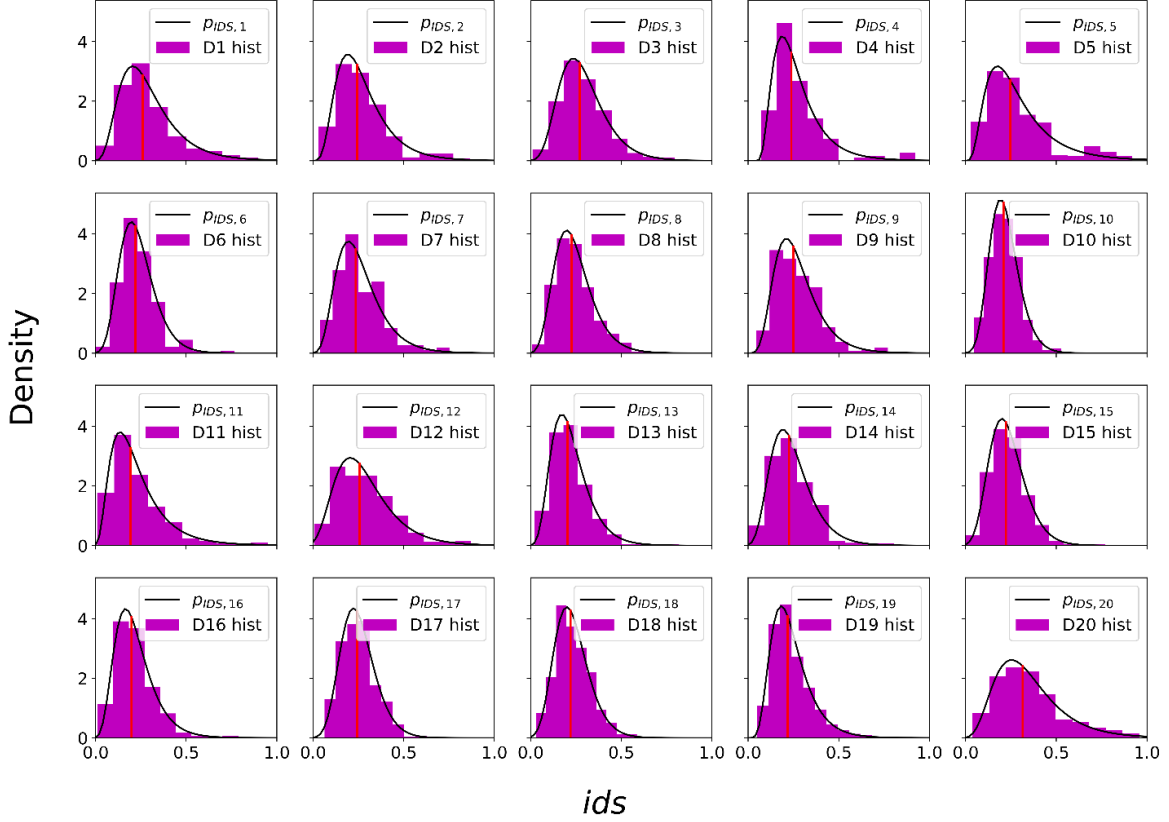


Figure 6. Histogram of the observed IDS values for each driver along with the fitted lognormal PDF. The vertical red lines denote the location of the median.

3.2 Inter-driver heterogeneity

With inter-driver heterogeneity, we refer to the difference in the driving styles among drivers. This heterogeneity is explored through the fitted PDF related to each driver. A visual inspection of the different driving behaviours is already visible from Figure 6. To facilitate microsimulation of driver heterogeneity in large-scale studies we performed an additional step clustering the 20 drivers into 3 categories using the simple K-means algorithm (Macqueen, 1967). The variables used for the K-means clustering refer to descriptive statistics of the lognormal PDFs. Three features used for that, one related to the central tendency of the PDF and another two related to the spread of the PDF (25th, 75th percentiles). The overall result of this stage is the creation of 3 different clusters represented by the specified clustering centres. Those centres represent three different drivers, namely a mild, a normal and a dynamic one.

To assess the clustering outcome, we use the two-sample K-S test. This is used initially to test whether two samples come from the same distribution, and the procedure is quite similar to the K-S test mentioned above. In this case, we use the two-sample K-S test to compare the PDFs of drivers in pairs. We generated a sample of 1.000.000 random values based on the PDF of each driver. The null hypothesis, in this case, is that the two samples come from the same distribution. The hypothesis is rejected if the test statistic D is more significant than a critical value obtained for the specific sample size and with a significance level of 1%. In our case, we know a priori that each pair of samples comes from different distributions, which is also confirmed by the test. The goal, however, is to assess how different the two distributions are. The resulting test statistic D indicates the maximum difference between the two cumulative density functions under consideration and this is the indicator used to compare the drivers' PDFs.

Figure 7 (a) presents the results of this grouping in the form of a 3D plot. The axes refer to the median, the 25th and the 75th percentile values. Drivers belonging to the same group are plotted with the same marker, while black points show the clustering centers which are the representatives of each group. One driver (D20) exhibited more significant differences to the rest of the drivers, which was also obvious in the visual inspection and constituted a separate group.

From the cluster centres, three types of drivers are deduced, a mild (cluster with triangular marker), a normal (cluster with round marker) and a more dynamic one (cluster with rhomb marker). The $p_{IDS,i}$ of each driver type is assigned with three percentiles, however, it is identified through its three parameters (shape, location, scale). In order to facilitate the reproduction of each driver by the reader, with the three known quantiles, one can analytically define the three parameters and infer the driver's PDF. This procedure is described in detail in Appendix Part E, which also reports the inferred parameters of the cluster centres. Figure 7 (b) presents the distribution per driver category. As expected, there is a large overlapping area between the different driver clusters. An aggressive driver is not expected to drive constantly in an aggressive way, as this is not always allowed, e.g. due to traffic state, weather, mood or other stochastic factors. The discrimination among them is clear though, in terms of the location of the mode (and consequently the median) as well as the range of values they cover. The distribution of mild drivers shows higher probability for lower IDS values than normal or aggressive ones. Furthermore, the distinguished characteristics of the different cluster are expected to become more apparent with more driving. For reference, later in the paper, Drivers with ids 6,7,10,11,13,15,16,18 and 19 are clustered as mild, drivers with ids 1,2,3,4,5,7,9,12 and 17 are clustered as normal and driver with id 20 is alone in aggressive cluster.

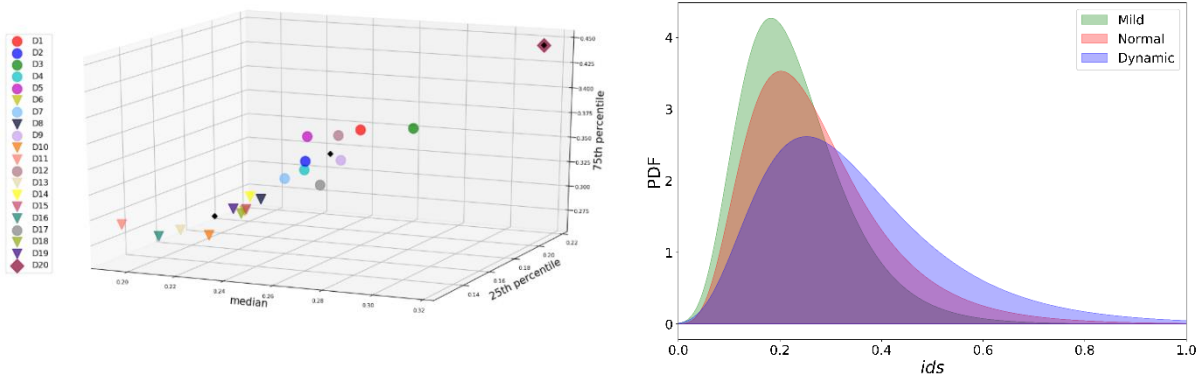


Figure 7. a) K-means clustering result presented in a 3D plot, b) PDFs of the inferred mild, normal and dynamic driver type.

Furthermore, Figure 8 summarises the results from the two-sample K-S test. This process is used as a tool to assess the clustering process. In each comparison, the null hypothesis is rejected, meaning that the two samples come from different distributions and the p-values being smaller than the significance level of 0.01 also support the rejection of the null hypothesis. The D-statistic reported in the color bar of Figure 8, reveals the magnitude of differences among drivers' Cumulative Distribution Functions; hence the smaller it is, the more similar the driving behaviours are. Colour-wise, the closer to purple, the more similar driving behaviours are considered. Additionally, annotations in the heat map reveal the K-means clustering results with **n**, **m**, referring to normal, mild driver cluster and **x** the fact that the compared pair of drivers were not assigned to the same group (keeping in mind that D20 constitutes the dynamic group).

For example, drivers with IDs: 1,2,3,4,5,7,9,12,17 are clustered as normal drivers. Looking the first row in Figure 8, i.e. D1, all the drivers from the same cluster have the notation “n”, i.e. normal. The colors signify their distribution similarity derived by the K-S test. Therefore, D1 is most similar with D12 and less similar with D17. It is obvious that the drivers from different clusters have less similarity (color-wise). Similar, D6

belongs to the mild cluster along with drivers with IDs: 6,7,10,11,13,15,16,18,19. Looking at the sixth row in the figure, the distribution of D6 is very similar (color-wise) with the distribution of the rest of the same-cluster drivers. Finally, D20 is the only truly dynamic driver, and his distribution is very different (colour-wise) from all the other 19 drivers.

To provide a quantitative representation of the results in Figure 8, the average D statistic values for mild, and normal cluster are 0.0723 and 0.0759 (the value for dynamic is zero since there is only one driver). In contrast, the average D statistic values between mild and normal is 0.148, between mild and dynamic 0.32 and between normal and dynamic 0.193. Therefore, the inferred clusters seem concise with high similarity scores (low D statistic values). The similarity score reduces between different clusters (higher D statistic values) and the lowest similarity is between mild and dynamic clusters, as expected.

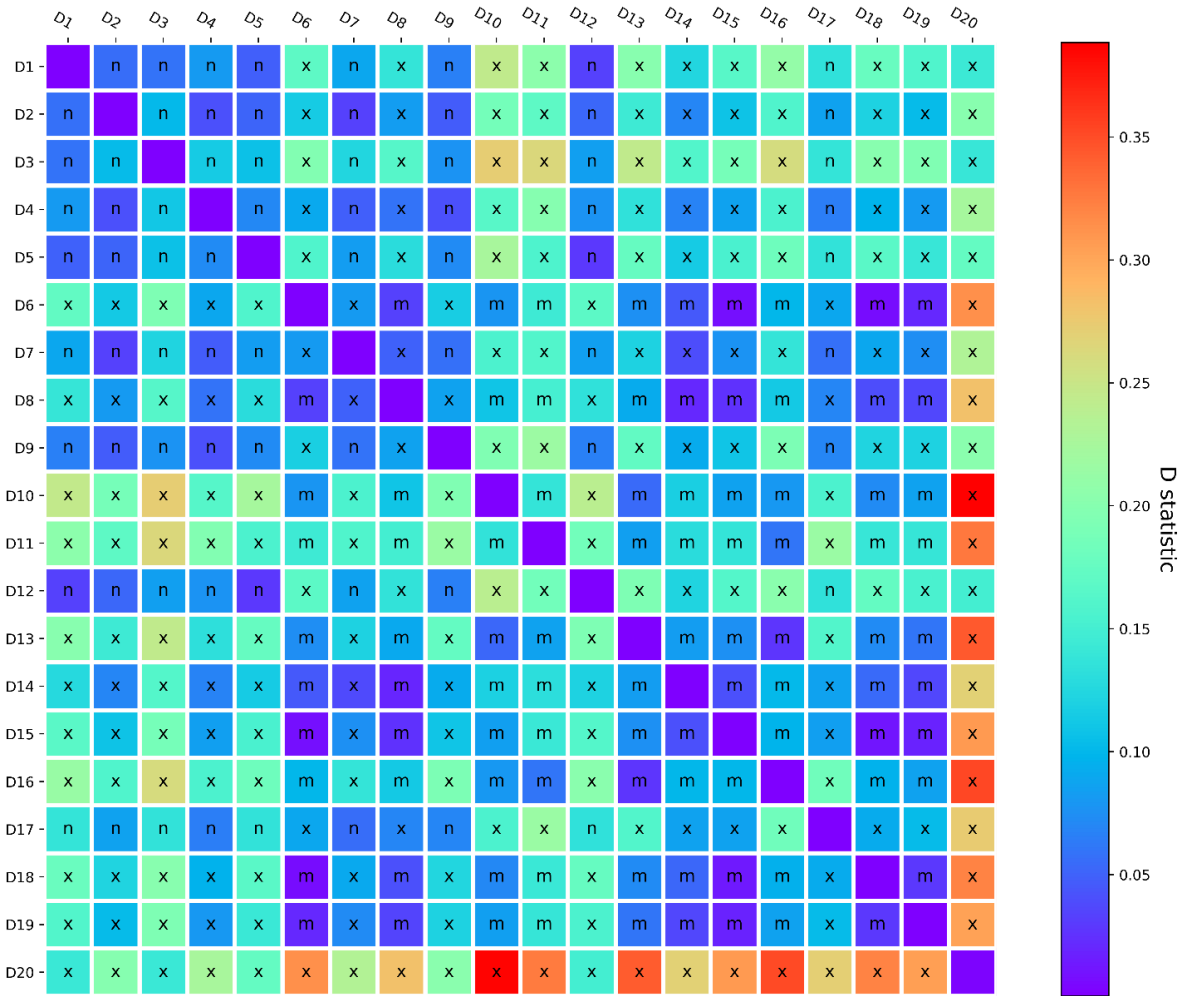


Figure 8. Result of the two-sample K-S test in the form of a heat map.

3.3 Intra-driver heterogeneity

Intra-driver heterogeneity refers to the different driving styles that a driver employs under various conditions. This kind of heterogeneity is assessed here since it is a crucial factor potentially affecting the observed variation in traffic-related variables such as headway (Li et al., 2020). An idea of the variation on the driving style of a single driver, is already taken by observing the fitted PDF. Its wideness visually shows which driver is more consistent with his driving style with respect to others.

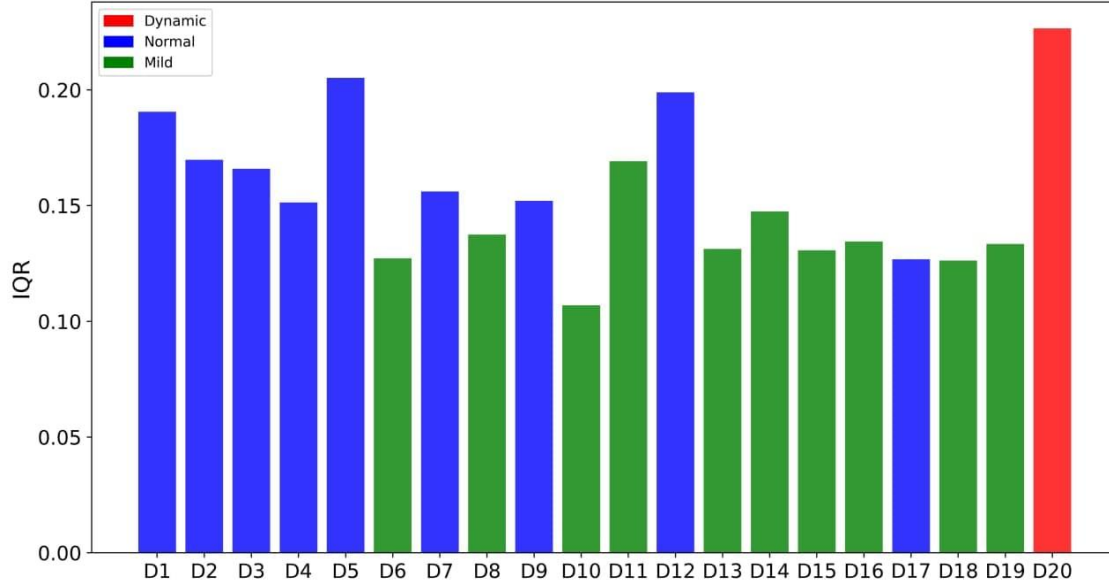


Figure 9. Bar plot of the IQR of the drivers' PDFs.

To quantitatively explore the intra-driver heterogeneity, we refer again to descriptive statistics. More specifically, we use a measure of statistical dispersion, the interquartile range (IQR), which is equal to the difference between 75th and 25th percentiles. Drivers with bigger IQR are considered to have a bigger degree of intra-driver heterogeneity. This heterogeneity is linked only to the different driving behaviours since the vehicle remains the same in all cases. Figure 9 illustrates the IQR values for each driver. Drivers D1, D5, D12 (normal cluster) and D20 (dynamic cluster) demonstrate the biggest IQR, and therefore largest intra-driver heterogeneity. Furthermore, as expected most mild drivers demonstrate low intra-driver heterogeneity, i.e. narrow IDS distributions. These quantitative results are aligned with expected empirical behaviours for mild, normal and dynamic drivers.

3.4 Driver simulation

The proposed model has been built on the MFC free-flow acceleration model (Makridis et al., 2019). MFC models the free-flow vehicle acceleration on the basis of the vehicle characteristics and the driver behaviour. For the first part it needs the vehicle specifications, i.e. mass, powertrain, torque etc., while for the second part it uses a constant parameter similar to the *ids* value described in the previous section. MFC can be incorporated in car-following models by replacing their free-flow component with it. Results from previous studies (Makridis et al., 2020a) have shown that adopting a simplified Lagrangian Godunov scheme (Leclercq et al., 2007) the MFC is able to reproduce macroscopically-observed phenomena with the formation and propagation of traffic oscillations in the absence of lane changes that can be explained by the stochastic nature of drivers' acceleration processes. Moreover, MFC supports the car-following model to reproduce the concave growth pattern of the speed standard deviation for a group of vehicles in car-platoon formation. Figure 10 illustrates the MFC behavior within the framework of the LWR model.

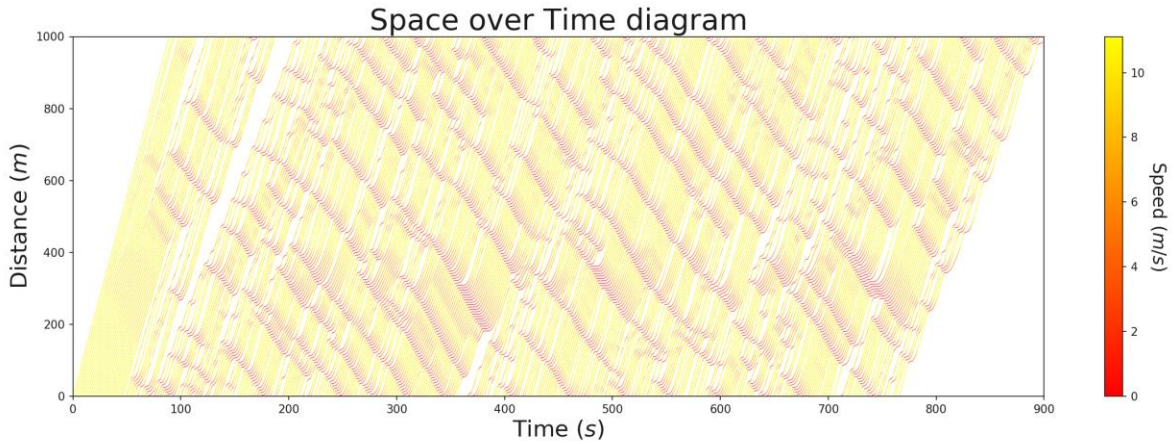


Figure 10. Reproduction of empirically-observed traffic oscillations with the MFC-LWR model as shown in (Makridis et al., 2020a).

In the previous work, though, each driver is simulated assuming constant behaviour across the whole simulation. In the present work, instead of using a constant driver behaviour parameter, we assume a distribution according to the PDF of instantaneous IDS values as described in the methodological part. Since the aim of this work is not on traffic oscillations, in this section, we provide validation results only on the new free-flow behaviour of the proposed model. However, it can be expected that the new model can produce oscillations of even more variable amplitudes and frequencies. Finally, the availability of mild, normal and dynamic driver distributions provided in this paper enables the incorporation of the model in large-scale simulation studies where the driver behaviour composition is unknown.

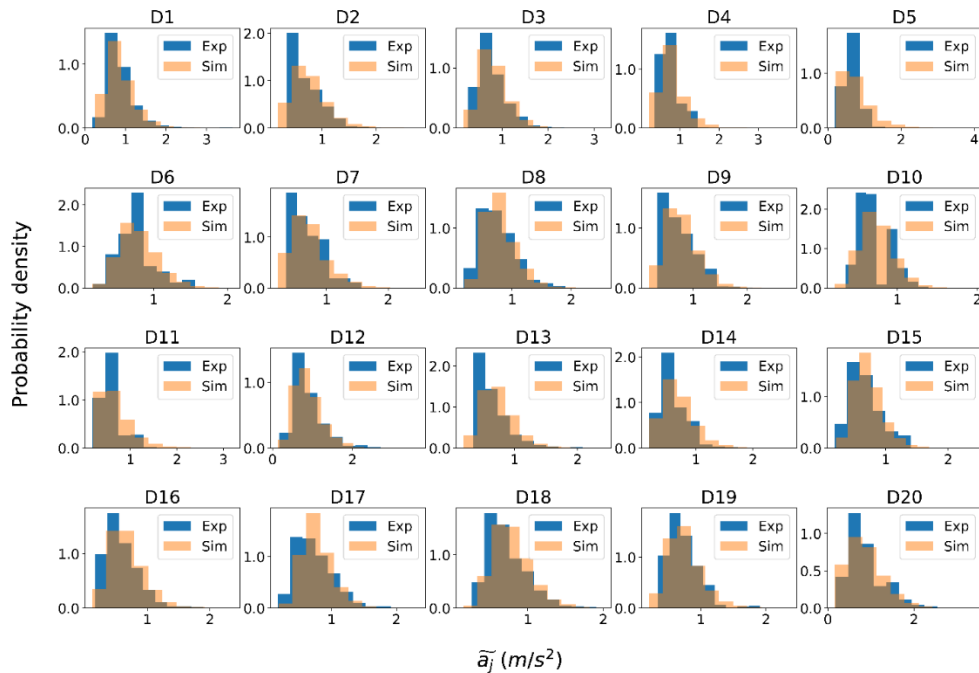


Figure 11. Median acceleration per event histograms of measured and simulated data.

The assessment of the proposed model to simulate different drivers is performed in two levels. First, all the events from all drivers are considered and simulated, i.e. acceleration from the low speed to the high speed of a certain event. Model-wise, each event is simulated based on a randomly sampled IDS value from the

respective PDF of each driver. For each event, we perform 10 simulations, each one with a different random IDS sample. To verify the results, simulated and experimentally-measured data are compared with regard to their median acceleration and median speed distributions per event (similar to the methodological development). Figures 11 and 12 illustrate the respective results, where stochastic simulations of the events based on specific PDFs capture the distribution for each specific driver very well. Practically, this means that assuming a large dataset of driver observations; the simulated driver will produce acceleration, speed and thus energy consumption values very close to real-world observations.

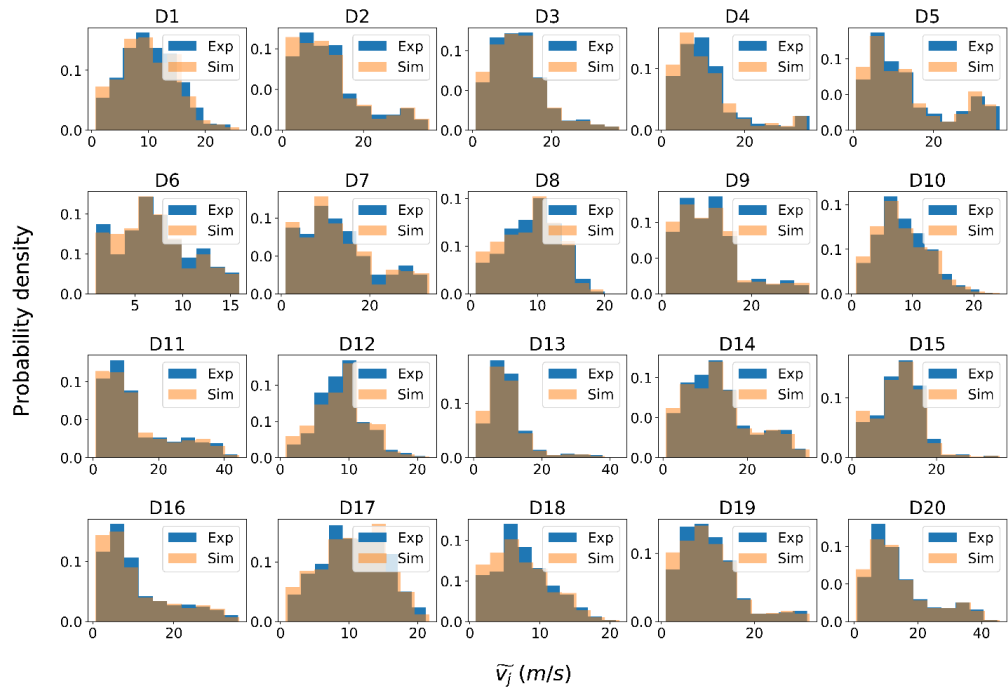


Figure 12. Median speed per event histograms of measured and simulated data.

Second, we demonstrate the model’s capability on the microscopic level of a single acceleration event. For each event of each driver we perform two simulations, one using the 25th percentile value of the driver’s PDF and a second considering the 75th percentile value from the same PDF. Figure 13 shows how empirical accelerations lie within the area inscribed by the two simulations. The results show one indicative acceleration event per driver but in general hold for all cases.

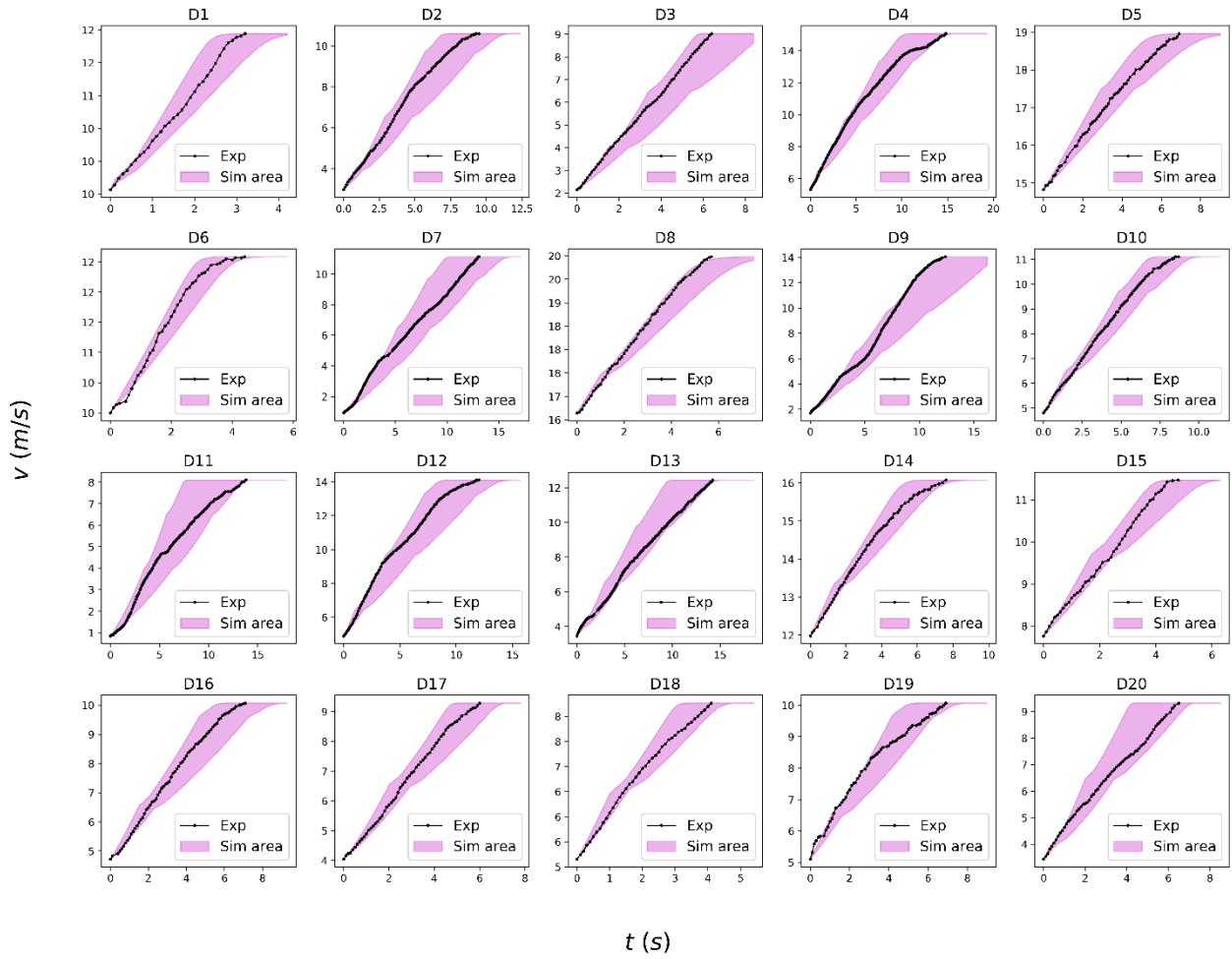


Figure 13. Demo of simulation of instantaneous measurements of speed over time.

In the last part, we simulated the three inferred driver clusters, i.e. mild, normal and aggressive, on the basis of a simple acceleration scenario. The scenario duration is 90 seconds. In the scenario the driver is requested to accelerate from standstill to a desired speed of 30 m/s . If the driver reaches the desired speed before the end of the scenario duration, the same speed is kept for the remaining time. We perform 1000 simulations with randomly selected IDS values from the cluster's PDF, i.e. 3000 simulations in total, and we provide comparative results.

Figure 14 shows histograms of median accelerations and median speeds for the simulated event per driver type. One can distinguish the different types of drivers. There are overlapping areas, as expected in real-world observations, meaning that their differences are more apparent in the regions of low and high accelerations.

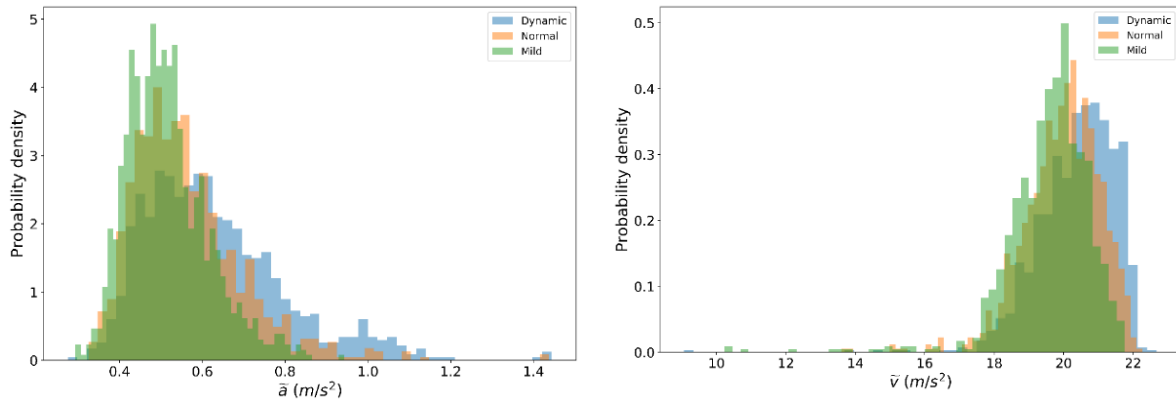


Figure 14. Histograms of median speed and median accelerations of the simulations concerning the three driver types.

Since the drivers' distributions overlap, we can expect that in certain simulations, the mild driver might accelerate faster than the normal or dynamic one. This is the desired property as it resembles the expected behaviour in real-world. In fact, Figure 15 shows a simulation example for all possible combinations between the three profiles. It is interesting to note how the lag between two consecutive drivers varies in each example. Finally, looking from a high-level analysis point of view, Table 2 presents the statistics of the occurrence of each simulation case. At the macroscopic level, we see the anticipated relationship between the profiles, i.e. in the majority of the cases, the dynamic driver is faster than the normal (61.5% - cases 1,2,6), and the mild one (70.1% - cases 1,2,3) and the mild driver is slower than that dynamic (70.1% - cases 1,2,3) and the normal one (59.5% - cases 1,3,4).

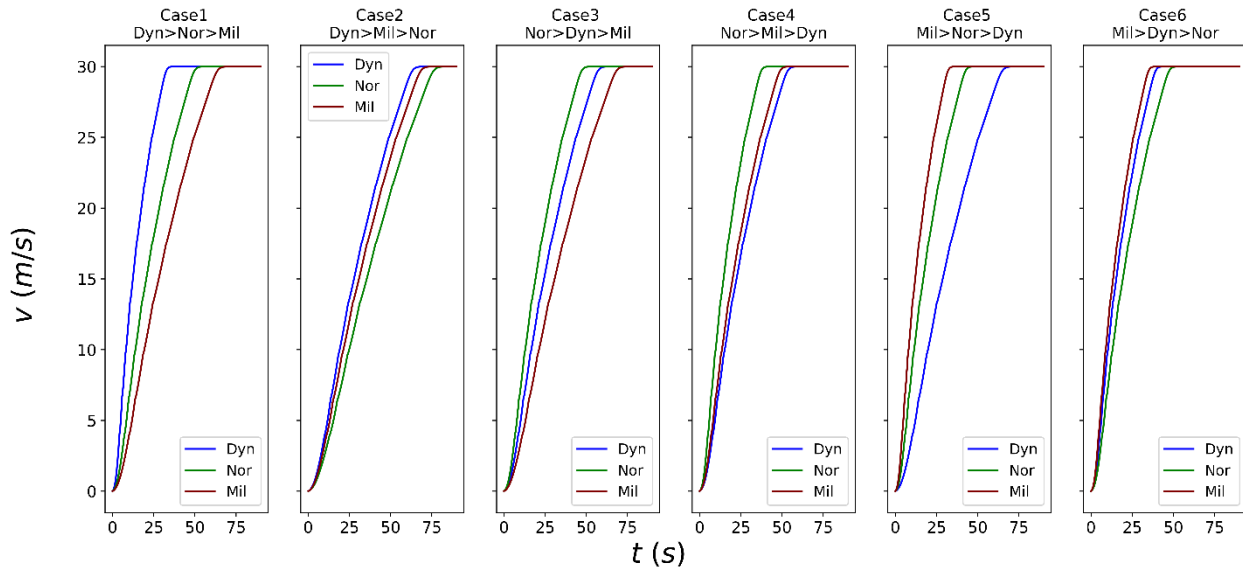


Figure 15. Speed over time plot of the simulated event related to the three driver types. 6 different cases are presented.

Table 2. Percentage of occurrence of each case.

<i>Cases</i>	<i>1</i>	<i>2</i>	<i>3</i>	<i>4</i>	<i>5</i>	<i>6</i>
<i>% of occurrence</i>	30.3	21.9	17.9	11.3	9.2	9.3

4 Conclusion

The present study proposes a novel framework to characterise driver behaviour based on the analysis of vehicle trajectories and provide an understanding on the driving style of an observed driver. The instantaneous acceleration is often a quantity that characterises the driver's aggressiveness in the literature. This paper argues that acceleration can be misleading for comparative driver analysis when the involved vehicles have very different power capabilities or the observations refer to mixed heterogeneous networks. A novel metric, called Independent Driving Style (IDS) that is invariant to the vehicle dynamics and the vehicle's speed, is proposed to tackle this problem. The proposed metric can be used for comparative analysis of the same driver in different vehicles, different drivers on the same vehicle or both and it is therefore considered suitable for an objective driving style description. Finally, the driver's behavioural fingerprint is conceptualised as a probability distribution of IDS values. A large experimental campaign with 20 drivers using interchangeably the same vehicle for a period of 1 year has been used in the present study to validate the proposed framework. The campaign is part of the OpenACC initiative (Makridis et al., 2020b) of the European Commission Joint Research Centre.

Finally, a way to extend the MFC free-flow driver model to incorporate both inter- and intra-driver heterogeneity in traffic simulation has been proposed and validated. In particular, the proposed approach employs each driver's derived IDS distribution to simulate a specific profile stochastically. Results demonstrate the robustness of the methodology and show that inter and intra-driver heterogeneity can be well captured by lognormal distributions of the instantaneous IDS values of the drivers. Furthermore, the paper suggests a simple classification of drivers into three prevalent groups (dynamic, ordinary and mild drivers) to facilitate easier driver-fleet reproduction in microscopic simulation software.

Future work will assess through large-scale experimental data, the capability of the proposed study to describe and differentiate the behavioural differences of automated driver assistance systems, as well as compare their behaviour with human drivers.

Acknowledgements

This research has been funded by the Joint Research Centre of the European Commission. The views expressed are purely those of the authors and may not, under any circumstances, be regarded as an official position of the European Commission. The authors are grateful to Vincenzo Arcidiacono for the help regarding CO₂MPAS gear identification tool and to Jelica Pavlovic and Kostis Anagnostopoulos for the help regarding the pre-processing of the experimental data. The views expressed in the paper are purely those of the authors and may not, under any circumstances, be regarded as an official position of the European Commission

References

- Antoniou, I., Ivanov, V.V, Ivanov, Valery V, Zrelov, P.V., 2002. On the log-normal distribution of network traffic. *Physica D: Nonlinear Phenomena* 167, 72–85. [https://doi.org/10.1016/S0167-2789\(02\)00431-1](https://doi.org/10.1016/S0167-2789(02)00431-1)
- Berthoume, A.L., James, R.M., Hammit, B.E., Foreman, C., Melson, C.L., 2018. Variations in Driver Behavior: An Analysis of Car-Following Behavior Heterogeneity as a Function of Road Type and Traffic Condition. *Transportation Research Record* 2672, 31–44. <https://doi.org/10.1177/0361198118798713>
- Calvert, S.C., van Arem, B., 2020. A generic multi-level framework for microscopic traffic simulation with automated vehicles in mixed traffic. *Transportation Research Part C: Emerging Technologies* 110, 291–311. <https://doi.org/10.1016/j.trc.2019.11.019>

- Chen, D., Ahn, S., Laval, J., Zheng, Z., 2014. On the periodicity of traffic oscillations and capacity drop: The role of driver characteristics. *Transportation Research Part B: Methodological* 59, 117–136. <https://doi.org/10.1016/j.trb.2013.11.005>
- Ciuffo, B., Makridis, M., Toledo, T., Fontaras, G., 2018. Capability of Current Car-Following Models to Reproduce Vehicle Free-Flow Acceleration Dynamics. *IEEE Transactions on Intelligent Transportation Systems* 19, 3594–3603. <https://doi.org/10.1109/TITS.2018.2866271>
- Fadhloun, K., Rakha, H., 2020. A novel vehicle dynamics and human behavior car-following model: Model development and preliminary testing. *International Journal of Transportation Science and Technology* 9, 14–28. <https://doi.org/10.1016/j.ijtst.2019.05.004>
- Fontaras, G., Valverde, V., Arcidiacono, V., Tsiakmakis, S., Anagnostopoulos, K., Komnos, D., Pavlovic, J., Ciuffo, B., 2018. The development and validation of a vehicle simulator for the introduction of Worldwide Harmonized test protocol in the European light duty vehicle CO2 certification process. *Applied Energy* 226, 784–796. <https://doi.org/10.1016/j.apenergy.2018.06.009>
- Gualandj, S., Toscani, G., 2019. Human behavior and lognormal distribution. A kinetic description. *Math. Models Methods Appl. Sci.* 29, 717–753. <https://doi.org/10.1142/S0218202519400049>
- Hamdar, S.H., Mahmassani, H.S., Treiber, M., 2015. From behavioral psychology to acceleration modeling: Calibration, validation, and exploration of drivers' cognitive and safety parameters in a risk-taking environment. *Transportation Research Part B: Methodological* 78, 32–53. <https://doi.org/10.1016/j.trb.2015.03.011>
- He, Y., Makridis, M., Mattas, K., Fontaras, G., Ciuffo, B., Xu, H., 2020. Introducing Electrified Vehicle Dynamics in Traffic Simulation. *Transportation Research Record* 2674, 776–791. <https://doi.org/10.1177/0361198120931842>
- Hoogendoorn, R.G., Hoogendoorn, S.P., Brookhuis, K.A., Daamen, W., 2011. Adaptation Longitudinal Driving Behavior, Mental Workload, and Psycho-Spacing Models in Fog. *Transportation Research Record* 2249, 20–28. <https://doi.org/10.3141/2249-04>
- Huang, Y.-X., Jiang, R., Zhang, H., Hu, M.-B., Tian, J.-F., Jia, B., Gao, Z.-Y., 2018. Experimental study and modeling of car-following behavior under high speed situation. *Transportation Research Part C: Emerging Technologies* 97, 194–215. <https://doi.org/10.1016/j.trc.2018.10.022>
- Laval, J.A., Leclercq, L., 2010. A mechanism to describe the formation and propagation of stop-and-go waves in congested freeway traffic. *Phil. Trans. R. Soc. A.* 368, 4519–4541. <https://doi.org/10.1098/rsta.2010.0138>
- Laval, J.A., Toth, C.S., Zhou, Y., 2014. A parsimonious model for the formation of oscillations in car-following models. *Transportation Research Part B: Methodological* 70, 228–238. <https://doi.org/10.1016/j.trb.2014.09.004>
- Leclercq, L., Laval, J.A., Chevallier, E., 2007. The Lagrangian Coordinates and What it Means for First Order Traffic Flow Models. Presented at the International Symposium on Transportation and Traffic Theory.
- Li, L., Jiang, R., He, Z., Chen, X. (Michael), Zhou, X., 2020. Trajectory data-based traffic flow studies: A revisit. *Transportation Research Part C: Emerging Technologies* 114, 225–240. <https://doi.org/10.1016/j.trc.2020.02.016>
- Macqueen, J., 1967. SOME METHODS FOR CLASSIFICATION AND ANALYSIS OF MULTIVARIATE OBSERVATIONS 5.1, 17.
- Makridis, M., Fontaras, G., Ciuffo, B., Mattas, K., 2019. MFC Free-Flow Model: Introducing Vehicle Dynamics in Microsimulation. *Transportation Research Record* 036119811983851. <https://doi.org/10.1177/0361198119838515>
- Makridis, M., Leclercq, L., Ciuffo, B., Fontaras, G., Mattas, K., 2020a. Formalizing the heterogeneity of the vehicle-driver system to reproduce traffic oscillations. *Transportation Research Part C: Emerging Technologies* 120, 102803.

- Makridis, M., Mattas, K., Anesiadou, A., Ciuffo, B., 2021. OpenACC. An open database of car-following experiments to study the properties of commercial ACC systems. *Transportation Research Part C: Emerging Technologies* 125.
- Makridis, M., Mattas, K., Anesiadou, A., Ciuffo, B., 2020b. OpenACC Database.
- Ngoduy, D., Lee, S., Treiber, M., Keyvan-Ekbatani, M., Vu, H.L., 2019. Langevin method for a continuous stochastic car-following model and its stability conditions. *Transportation Research Part C: Emerging Technologies* 105, 599–610. <https://doi.org/10.1016/j.trc.2019.06.005>
- Ossen, S., Hoogendoorn, S.P., 2011. Heterogeneity in car-following behavior: Theory and empirics. *Transportation Research Part C: Emerging Technologies, Emerging theories in traffic and transportation and methods for transportation planning and operations* 19, 182–195. <https://doi.org/10.1016/j.trc.2010.05.006>
- Pavlovic, J., Fontaras, G., Ktistakis, M., Anagnostopoulos, K., Komnos, D., Ciuffo, B., Clairotte, M., Valverde, V., 2020. Understanding the origins and variability of the fuel consumption gap: lessons learned from laboratory tests and a real-driving campaign. *Environmental Sciences Europe* 32, 53. <https://doi.org/10.1186/s12302-020-00338-1>
- Punzo, V., Borzacchiello, M.T., Ciuffo, B., 2011. On the assessment of vehicle trajectory data accuracy and application to the Next Generation SIMulation (NGSIM) program data. *Transportation Research Part C: Emerging Technologies* 19, 1243–1262. <https://doi.org/10.1016/j.trc.2010.12.007>
- Rakha, H., Snare, M., Dion, F., 2004. Vehicle Dynamics Model for Estimating Maximum Light-Duty Vehicle Acceleration Levels. *Transportation Research Record* 1883, 40–49. <https://doi.org/10.3141/1883-05>
- Rakha, H.A., Ahn, K., Faris, W., Moran, K.S., 2012. Simple Vehicle Powertrain Model for Modeling Intelligent Vehicle Applications. *IEEE Trans. Intell. Transport. Syst.* 13, 770–780. <https://doi.org/10.1109/TITS.2012.2188517>
- Saifuzzaman, M., Zheng, Z., Haque, Md.M., Washington, S., 2017. Understanding the mechanism of traffic hysteresis and traffic oscillations through the change in task difficulty level. *Transportation Research Part B: Methodological* 105, 523–538. <https://doi.org/10.1016/j.trb.2017.09.023>
- Singh, V.P., 1998. Three-Parameter Lognormal Distribution, in: *Entropy-Based Parameter Estimation in Hydrology*. Springer Netherlands, Dordrecht, pp. 82–107. https://doi.org/10.1007/978-94-017-1431-0_7
- Spearman, C., 1904. The Proof and Measurement of Association between Two Things. *The American Journal of Psychology* 15, 72–101. <https://doi.org/10.2307/1412159>
- Taylor, J., Zhou, X., Roupail, N.M., Porter, R.J., 2015. Method for investigating intradriver heterogeneity using vehicle trajectory data: A Dynamic Time Warping approach. *Transportation Research Part B: Methodological* 73, 59–80. <https://doi.org/10.1016/j.trb.2014.12.009>
- Treiber, M., Kesting, A., 2013. *Traffic Flow Dynamics*. Springer Berlin Heidelberg, Berlin, Heidelberg. <https://doi.org/10.1007/978-3-642-32460-4>
- Treiber, M., Kesting, A., Helbing, D., 2006. Delays, inaccuracies and anticipation in microscopic traffic models. *Physica A: Statistical Mechanics and its Applications* 360, 71–88. <https://doi.org/10.1016/j.physa.2005.05.001>
- Wang, H., Wang, W., Chen, J., Jing, M., 2010. Using Trajectory Data to Analyze Intradriver Heterogeneity in Car-Following. *Transportation Research Record* 2188, 85–95. <https://doi.org/10.3141/2188-10>
- Zhao, X., Wang, Z., Xu, Z., Wang, Y., Li, X., Qu, X., 2020. Field experiments on longitudinal characteristics of human driver behavior following an autonomous vehicle. *Transportation Research Part C: Emerging Technologies* 114, 205–224. <https://doi.org/10.1016/j.trc.2020.02.018>
- Zheng, Z., Ahn, S., Chen, D., Laval, J., 2011. Freeway traffic oscillations: Microscopic analysis of formations and propagations using Wavelet Transform. *Transportation Research Part B: Methodological* 45, 1378–1388. <https://doi.org/10.1016/j.trb.2011.05.012>

Appendix

Part A - Fitted curves defining the operational domain in median *DS*-median Speed space

Table A.1 Characteristics of fitted curves along with the special conditions for each one.

Curve	Polynomial curves	Special conditions
f_{min}	$f_{min}(\tilde{v}) = 0.009 \cdot \tilde{v} - 0.009$	$f_{min}(\tilde{v}) \geq \text{Min } \widetilde{ds}_{exp}$
f_{max}	$f_{max}(\tilde{v}) = 3.70 \cdot 10^{-5} \tilde{v}^3 - 0.003 \tilde{v}^2 + 0.084 \cdot \tilde{v} + 0.167$	

Where $\text{Min } \widetilde{ds}_{exp}$ is the minimum observed median *ds* value equal to 0.021, \tilde{v} is the median speed value.

Part B - Relationship of \tilde{a} , \widetilde{ds} and *ids* per event versus \tilde{v}

To showcase the relationship of the \tilde{v}_j , \widetilde{ds}_j and *ids*_{*j*} with \tilde{v}_j with *j* denoting the event, the Spearman rank-order correlation coefficient (Spearman, 1904) is computed. Spearman correlation is a nonparametric measure of the monotonic relationship between two datasets not necessarily normally distributed. The test provides the spearman correlation coefficient value which lies in the space $[-1,1]$ with 0 implying no correlation. The two-sided *p* – value is also provided, for a hypothesis test whose null hypothesis is that two sets of data are uncorrelated. In Table B.1, the results of the Spearman rank correlation are presented. In all cases, *p* – value is zero which denotes the fact that the results are statistically significant and there is much evidence to reject the null hypothesis and consider that in each case the pair of variables compared are correlated. The Spearman correlation values, reveal the evolution from the vehicle dependent and weakly to speed correlated median acceleration feature, to the vehicle independent and strongly correlated to speed \widetilde{ds}_j and finally to the weakly correlated to speed *ids*_{*j*} metric.

Table B.1. Spearman correlation test between median speed - median *ds* and median speed - *ids* per event.

Variables	\tilde{a}_j	\widetilde{ds}_j	<i>ids</i> _{<i>j</i>}	
\tilde{v}_j	Spearman Correlation	-0.306	0.818	0.248
	p-value. (2-tailed)	0.000	0.000	0.000
	N	14651	14651	14651

Part C - Goodness of fit K-S test of all drivers

Table C1 shows the results of the goodness of fit K-S test of all the $p_{IDS,i}$ functions. In all driver cases, the test statistic value was smaller than the critical value ($D < \text{Critical}$) which allows us not to reject the null hypothesis and accept, with a 1% level of significance, that all *ids*_{*i,j*} distributions can be represented by the inferred $p_{IDS,i}S$. Additionally, the resulting p-values were larger than the significance level (p-values \gg significance level), providing more evidence on not rejecting the null hypothesis.

Table C.1 The goodness of fit test results based on the K-S method.

Driver	Critical value	D statistic	p-value	Driver	Critical value	D statistic	p-value
D1	0.061	0.037	0.280	D11	0.080	0.019	0.999
D2	0.077	0.032	0.739	D12	0.076	0.036	0.596
D3	0.031	0.013	0.710	D13	0.043	0.019	0.662
D4	0.109	0.042	0.822	D14	0.051	0.032	0.264
D5	0.074	0.040	0.404	D15	0.070	0.023	0.928
D6	0.123	0.067	0.391	D16	0.053	0.035	0.188
D7	0.132	0.048	0.870	D17	0.065	0.026	0.768
D8	0.050	0.015	0.969	D18	0.066	0.024	0.859
D9	0.065	0.036	0.396	D19	0.088	0.035	0.782
D10	0.074	0.039	0.435	D20	0.048	0.022	0.662

Part D - Parameters of the lognormal PDFs of all drivers

A three-parameter lognormal PDF $p_{IDS,i}$ (Singh, 1998), with i being the driver id, is fitted at each one of them and shown as a black curve in the figure. The first parameter (shape) denotes the general form-shape of the distribution and is also equal to the standard deviation of the $\ln(ids_{i,j} - location)$, the second one (location) reveals the shift on the x-axis, representing a lower bound and the last one if combined with the shift parameter (scale + location) expresses the median of the $p_{IDS,i}$. For completion, Appendix C includes the parameters of the inferred $p_{IDS,i}$. The location of the median for each $p_{IDS,i}$ is denoted with a vertical red line in the figure.

Table D.1 presents the lognormal parameters which actually characterise the drivers. One can see that in most cases location parameters are slightly negative which means there is a tiny probability that the PDF takes negative values (more specifically, among all probabilities for an $p_{IDS,i}$ to get values smaller or equal to zero, the biggest one is 0.17%). At this stage we also note that those parameters do mathematically reconstruct each $p_{IDS,i}$, however, they do not directly reveal meaningful information for the lognormal itself, apart from the location shift. Therefore, descriptive statistics of each $p_{IDS,i}$ are used to analyse further the drivers' characteristics.

Table D.1 Parameters of the lognormal PDFs.

Driver	shape	location	scale	Driver	shape	location	scale
D1	0.448	-0.051	0.311	D11	0.560	-0.025	0.219
D2	0.456	-0.030	0.272	D12	0.383	-0.124	0.381
D3	0.312	-0.120	0.392	D13	0.355	-0.067	0.272
D4	0.529	0.031	0.208	D14	0.334	-0.099	0.324
D5	0.575	-0.011	0.258	D15	0.238	-0.182	0.405
D6	0.265	-0.132	0.353	D16	0.369	-0.068	0.267
D7	0.382	-0.064	0.300	D17	0.207	-0.211	0.452
D8	0.298	-0.113	0.340	D18	0.228	-0.189	0.409
D9	0.378	-0.046	0.295	D19	0.400	-0.026	0.244
D10	0.211	-0.166	0.375	D20	0.410	-0.089	0.405

Part E - Inferring a driver's PDF from the three parameters of a lognormal based on three percentiles

In this section, the analytical way of extracting the three parameters of the lognormal PDF (shape, loc, scale) based on its three quantiles (Q_{25}, Q_{50}, Q_{75}) is presented.

Quantile function of a regular lognormal PDF:

$$Quantile = e^{(\mu + \sigma\sqrt{2} \operatorname{erf}^{-1}(2p-1))} \quad E.1$$

For the three parameter lognormal PDF D.1 is slightly transformed as:

$$Quantile = e^{(\mu + \sigma\sqrt{2} \operatorname{erf}^{-1}(2p-1))} + loc \quad E.2$$

Where: $\mu = \ln(\text{scale})$, $\sigma = \text{shape}$, erf^{-1} = inverse error function, p = the respective percentiles, i.e: 0.25, 0.50, 0.75.

Therefore, by applying E.2, we have the following three equations:

$$Q_{25} = e^{(\mu + \sigma\sqrt{2} \operatorname{erf}^{-1}(2 \cdot 0.25 - 1))} + loc = e^{(\mu + \sigma\sqrt{2} \operatorname{erf}^{-1}(-0.5))} + loc \quad E.3$$

$$Q_{50} = e^{(\mu + \sigma\sqrt{2} \operatorname{erf}^{-1}(2 \cdot 0.5 - 1))} + loc = e^{(\mu + \sigma\sqrt{2} \operatorname{erf}^{-1}(0))} + loc \quad E.4$$

$$Q_{75} = e^{(\mu + \sigma\sqrt{2} \operatorname{erf}^{-1}(2 \cdot 0.75 - 1))} + loc = e^{(\mu + \sigma\sqrt{2} \operatorname{erf}^{-1}(0.5))} + loc \quad E.5$$

Where: $\operatorname{erf}^{-1}(-0.5) = -\operatorname{erf}^{-1}(0.5) \approx -0.477$ and $\operatorname{erf}^{-1}(0) = 0$

Combining E.3, E.4, E.5 and the values of the respective inverse error functions, we have:

$$Q_{25} = e^{(\mu + \sigma\sqrt{2} \operatorname{erf}^{-1}(-0.5))} + loc = e^{(\mu - 0.477\sigma\sqrt{2})} + loc \quad E.6$$

$$Q_{50} = e^{(\mu + \sigma\sqrt{2} \operatorname{erf}^{-1}(0))} + loc = e^{\mu} + loc \rightarrow loc = Q_{50} - e^{\mu} \quad E.7$$

$$Q_{75} = e^{(\mu + \sigma\sqrt{2} \operatorname{erf}^{-1}(2 \cdot 0.75 - 1))} + loc = e^{(\mu + 0.477\sigma\sqrt{2})} + loc \quad E.8$$

Therefore, we have three knowns Q_{25}, Q_{50}, Q_{75} and three unknowns σ, loc, μ .

Combining E.6, E.7 and E.8, we have:

$$e^{(\mu - 0.477\sigma\sqrt{2})} - e^{\mu} = Q_{25} - Q_{50} \rightarrow e^{\mu}(e^{(-0.477\sigma\sqrt{2})} - 1) = Q_{25} - Q_{50} \quad E.9$$

$$e^{(\mu + 0.477\sigma\sqrt{2})} - e^{\mu} = Q_{75} - Q_{50} \rightarrow e^{\mu}(e^{(+0.477\sigma\sqrt{2})} - 1) = Q_{75} - Q_{50} \quad E.10$$

Dividing E9 with E10:

$$\frac{e^{(-0.477\sigma\sqrt{2})} - 1}{e^{(+0.477\sigma\sqrt{2})} - 1} = \frac{Q_{25} - Q_{50}}{Q_{75} - Q_{50}} \quad E.11$$

We substitute

$$x = e^{(+0.477\sigma\sqrt{2})}, \text{ therefore: } e^{(-0.477\sigma\sqrt{2})} = \frac{1}{x}$$

Also, for convenience we substitute $\frac{Q_{25} - Q_{50}}{Q_{75} - Q_{50}} = c$

Taking these into account, in combination with E11 we end up with:

$$\frac{\frac{1}{x} - 1}{x - 1} = c \rightarrow \frac{1 - x}{x(x - 1)} = c \rightarrow \frac{1 - x}{x(x - 1)} = c \rightarrow cx^2 + (1 - c)x - 1 = 0 \quad E.12$$

E12 can be easily solved and the solutions are well-known:

$$cx^2 + (1 - c)x - 1 = 0 \rightarrow x = \frac{-(1 - c) \pm \sqrt{(1 - c)^2 - 4c(-1)}}{2c} \rightarrow$$

$$e^{(+0.477\sigma\sqrt{2})} = \frac{-(1-c) \pm \sqrt{(1-c)^2 - 4c(-1)}}{2c} \rightarrow$$

$$\sigma = \frac{\ln\left(\frac{-(1-c) \pm \sqrt{(1-c)^2 - 4c(-1)}}{2c}\right)}{0.447\sqrt{2}} \quad \text{E.13}$$

E13 provides two possible solutions for σ . To continue with the next unknowns, we subtract E.6 from E.8:

$$Q_{25} - Q_{75} = e^{(\mu - 0.477\sigma\sqrt{2})} + loc - e^{(\mu + 0.477\sigma\sqrt{2})} - loc \rightarrow$$

$$Q_{25} - Q_{75} = e^{(\mu - 0.477\sigma\sqrt{2})} - e^{(\mu + 0.477\sigma\sqrt{2})} = e^{\mu} (e^{-0.477\sigma\sqrt{2}} - e^{+0.477\sigma\sqrt{2}}) \rightarrow$$

$$e^{\mu} = \frac{Q_{25} - Q_{75}}{e^{-0.477\sigma\sqrt{2}} - e^{+0.477\sigma\sqrt{2}}} \xrightarrow{e^{\mu} = scale}$$

$$scale = \frac{Q_{25} - Q_{75}}{e^{-0.477\sigma\sqrt{2}} - e^{+0.477\sigma\sqrt{2}}} \quad \text{E.14}$$

E14 provides two possible solutions for *scale* since there are two possible solutions for σ .

Finally, from E7 there are also two possible solutions for the *loc* parameter:

$$loc = Q_{50} - \frac{Q_{25} - Q_{75}}{e^{-0.477\sigma\sqrt{2}} - e^{+0.477\sigma\sqrt{2}}} \quad \text{E.15}$$

After solving the equations numerically, one can easily reject one of the two possible solutions for the derived parameters shape, loc, scale since they provide unrealistic results.

Table E.1 shows the parameters to reproduce the PDFs for mild, normal and aggressive driver clusters.

Table E.1 Parameters of the lognormal PDFs of the different driver types.

Driver type	shape	location	scale
Mild	0.335	-0.081	0.295
Normal	0.416	-0.047	0.296
Dynamic	0.410	-0.089	0.405